Ion-Neutralization Spectroscopy of Copper and Nickel

H. D. HAGSTRUM AND G. E. BECKER
Bell Telephone Laboratories, Murray Hill, New Jersey
(Received 27 January 1967)

Experimental results concerning the band structure of copper and nickel have been obtained by a new method of electronic spectroscopy of solids. The spectroscopic information comes from deconvolution of the kinetic-energy distribution of electrons ejected in the radiationless, two-electron neutralization of slowly moving noble-gas ions at the solid surface. This leads to a transition density function which includes information about the density of states in the filled conduction band, transition probabilities of the Auger-type neutralization process, and possible many-body effects and final-state interactions. Data are presented for the atomically clean (111), (110), and (100) faces of both Cu and Ni, and for the ions He^+, Ne^+, and Ar^+. Transition probability factors depending on band energy, symmetry character of the band electron's wave function, and crystallographic orientation are evident in the results. The data are entirely consistent with the rigid-band model. Measurements above and below the Curie point for Ni are consistent with a spin-exchange energy of, at most, a few tenths of an eV. The large resonance centered at 4.5 eV below the Fermi level reported by photoelectric emission is not observed in this work. The same statement can be made concerning the resonance reported for Cu at 6 eV below the Fermi level. Detailed comparison is made with the results of band-structure calculations and with the experimental results from photoelectric emission and the soft-x-ray spectroscopy.

I. INTRODUCTION

IN this paper we present the first complete report of experimental results obtained by the method of ion-neutralization spectroscopy of solids (INS). These data concern the metals copper and nickel. Considerable interest now centers on the band structures of the noble and transition metals and on the questions of the validity of the rigid-band model and the nature of relatively deep-lying, many-body resonances. The present results cast light on both of these matters. A brief report of some of the present results has been published.[1] An extensive discussion of the method of INS has also been published.[2] Reference to this latter work is made repeatedly in this paper.

INS is a deep-band spectroscopy capable of investigating a filled band to a depth of 10 eV or more below the vacuum level. As such, it is comparable to the soft-x-ray spectroscopy (SXS) and the photoelectron spectroscopy (PES) based on photoemission. Both Cu and Ni have been studied by these other methods. Because each of the deep-band spectroscopies has its own peculiar transition-probability dependences, intercomparison of the results with the present work is enlightening. Also, theory has produced results with which experimental work may fruitfully be compared.

The plan of the present paper is as follows: A brief resumé of the method of INS is given in Sec. II, in which is included a more detailed discussion of energy resolution than has been given heretofore. Specific experimental conditions are detailed in Sec. III. The results for nickel and copper are presented in Secs. IV and V, respectively. Discussion of the INS results for Ni and Cu and comparison with the results of other deep-band spectroscopies and band-structure theory are to be found in Sec. VI.

II. BRIEF RESUMÉ OF THE METHOD OF INS

Ion-neutralization spectroscopy derives "spectroscopic" information about the solid from the kinetic-energy distributions of electrons ejected from the solid when an ion is neutralized at the surface. The measurement is made using the apparatus of Fig. 1 with the target T placed in the ion-neutralization apparatus at port 1. Here a focused, monoenergetic beam of slow ions (4–10 eV) strikes the target. Ejected electrons are collected on the spherical electrode S. The electron kinetic-energy distribution $X_K(E)$, for ions of incident kinetic energy K, is obtained as the differential of the curve of current to S versus retarding potential V_{ST} between S and T. Processing of the target at port 2 and its inspection by low-energy electron diffraction at port 3 are discussed in Sec. III.

The data presented in this paper are the first to be obtained with the apparatus of Fig. 1. The reader is referred to discussions of the design and use of earlier apparatus.[3,4] An experimental study of ion neutralization at one face of nickel, atomically clean Ni (111), using an earlier apparatus, has been published.[5] No attempt to use these data for the purposes of INS was then made. Data for Ni (111) have been obtained again in this work using a different sample in a different apparatus and the results are identical to those obtained earlier. Some comparison of the experimental conditions in these two experiments is made in Sec. III.

$X_5(E)$ distributions for 5-eV He^+, Ne^+, and Ar^+ ions incident on atomically clean Cu (111) are shown in Fig. 2. Similar data for the clean Cu (110) face were published in Fig. 2 of Ref. 2. Distributions for He^+ ions incident on three different crystallographic faces of nickel are

[1] H. D. Hagstrum and G. E. Becker, Phys. Rev. Letters **16**, 230 (1966).
[2] H. D. Hagstrum, Phys. Rev. **150**, 495 (1966).
[3] H. D. Hagstrum, Rev. Sci. Instr. **24**, 1122 (1953).
[4] H. D. Hagstrum, D. D. Pretzer, and Y. Takeishi, Rev. Sci. Instr. **36**, 1183 (1965).
[5] Y. Takeishi and H. D. Hagstrum, Phys. Rev. **137**, A641 (1965).

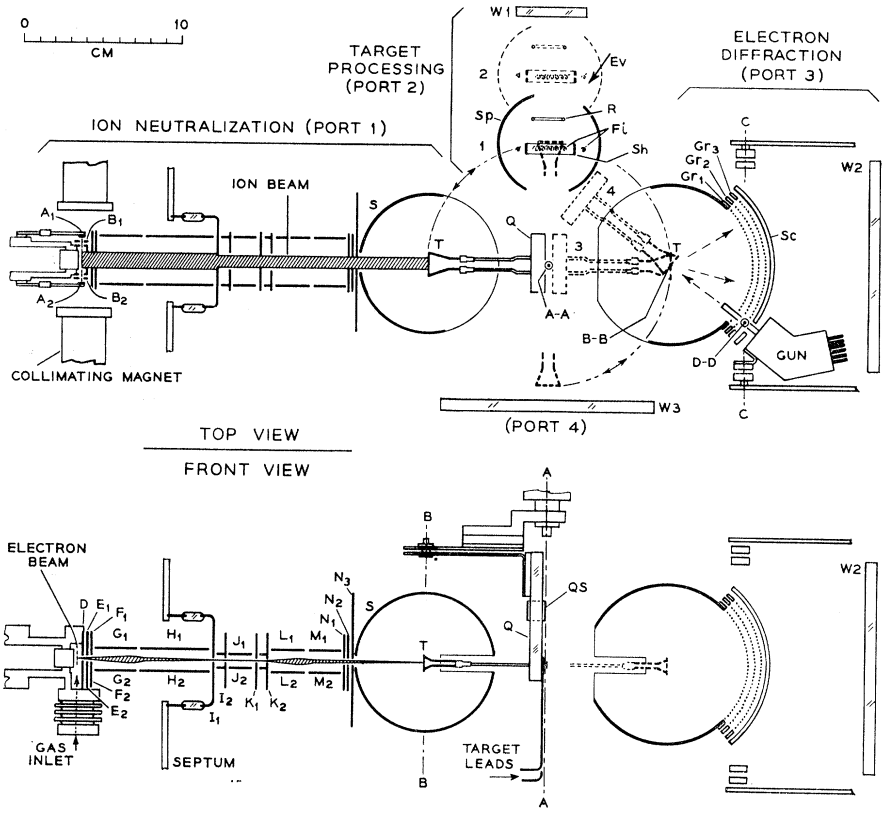

FIG. 1. Schematic diagram of experimental apparatus used. The target can be rotated about the vertical axis A-A and made to face each of four ports in a horizontal plane. Electrodes are labeled for reference in the text. W_1, W_2, and W_3 are glass windows. The arrow Ev indicates the direction from which material can be evaporated onto the target surface when the target faces port 2.

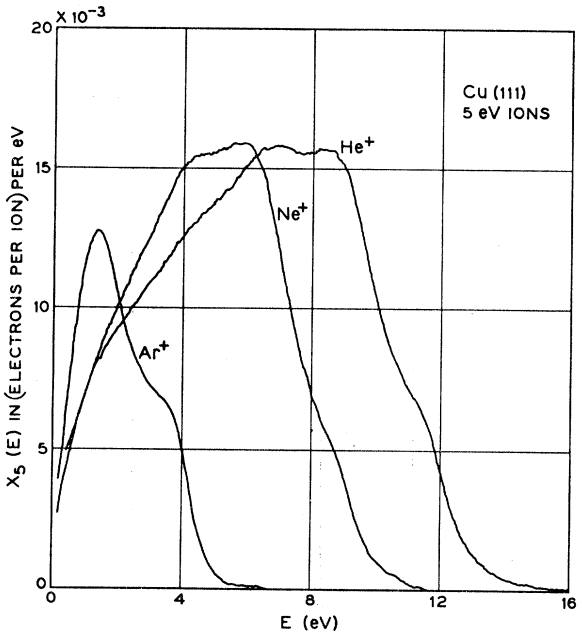

FIG. 2. Energy distributions of electrons ejected from atomically clean Cu (111) by 5 eV He^+, Ne^+, and Ar^+ ions. E is the energy above the vacuum level which is located by extrapolation of the curves to zero at the low-energy end. E differs from the experimentally measured voltage V_{ST} between sphere S and target T by the contact potential between S and T.

shown in Fig. 3. It is evident that $X_K(E)$ is dependent on the nature of the solid, the crystallographic face used, and the character of the incident ion. Data

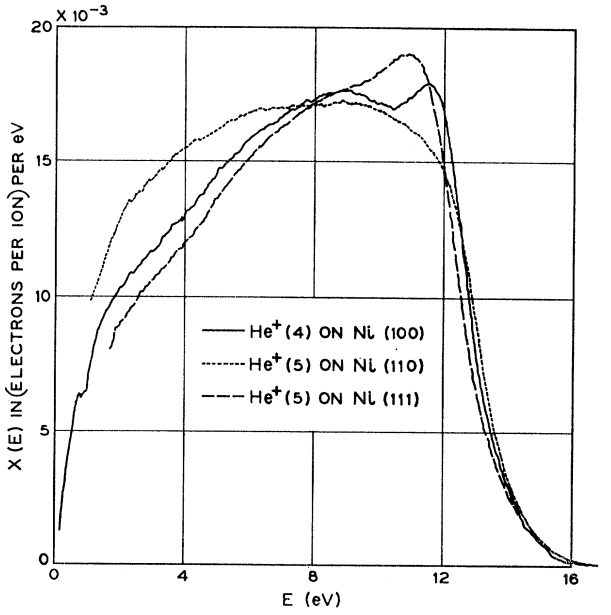

FIG. 3. Energy distributions of electrons ejected from the (100), (110), and (111) atomically clean faces of nickel by He^+ ions of 4-, 5-, and 5-eV incident kinetic energy, respectively.

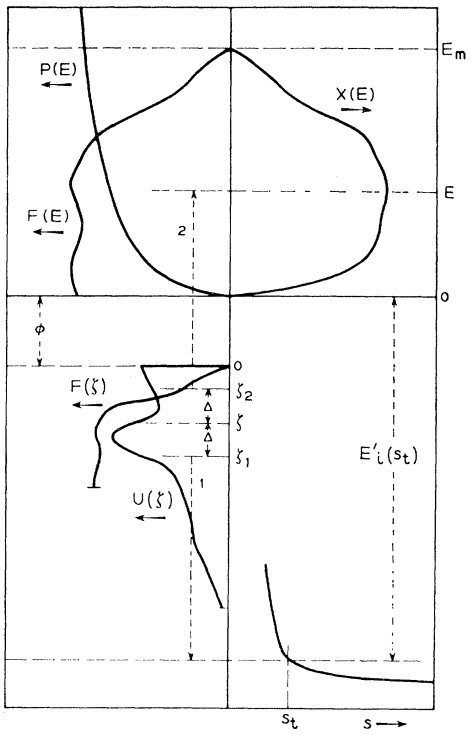

FIG. 4. Energy-level diagram defining energies and showing functions of energy related to the ion-neutralization process. The functions U, F, P, and X, defined in the text, are those for Cu (111). The variation of the atomic level, $E_i'(s)$, with distance s from the solid surface has been discussed in previous publications (Refs. 7 and 8). s_t is the position of the ion when the Auger neutralization process occurs. This figure defines the E and ζ energy scales.

showing the changes in the $X_K(E)$ distribution resulting from increased energy broadening as incident-ion energy K is increased have been presented in previous publications.[5,6]

The electronic transitions and the basic functional dependences of the ion-neutralization process are shown in Fig. 4. These have been discussed in detail in previous interpretative papers.[2,7,8] Two electrons in the filled band at energies ζ_1 and ζ_2 are involved in the radiationless, Auger-type process. One electron (1) tunnels into the atomic well and drops to the vacant level in the ion $E_i'(s_t)$ below the vacuum level, while the second (2) rises on the energy scale to become a fast internal secondary which may leave the solid. The energy distribution inside the solid of these excited electrons is $F(E)$ of Fig. 4. The probability that these electrons will escape through the surface of the solid is $P(E)$, also plotted in Fig. 4. The product $P(E)F(E)$ is equal to $X(E)$, the electron kinetic-energy distribution outside the solid which is determined experimentally.

If we assume provisionally that transition probability is independent of band energy, initial state k vector, symmetry character of the band state, and possible many-body effects and final-state interactions, it is easy to see the relation between $F(E)$ and the state density in the filled band, which is the function $U(\zeta)$ under the above assumptions. All processes involving pairs of electrons symmetrically disposed (Δ up and Δ down) with respect to that energy ζ which lies halfway between a given final-state energy E and the atomic ground state at $-E_i'$ will produce excited electrons at E. Assuming transition probability to depend on the density of states at $\zeta_1=\zeta+\Delta$ and $\zeta_2=\zeta-\Delta$, $F(E)$ should depend on the integral fold or self-convolution of $U(\zeta)$ as follows:

$$F(E)=F[E_i'-2(\zeta+\varphi)]=\int_0^{\zeta} U(\zeta+\Delta)U(\zeta-\Delta)d\Delta. \quad (1)$$

The relation between the variables E and ζ is found by equating the lengths of the vectors for the transitions 1 and 2. A $U(\zeta)$ function for copper and its fold $F(\zeta)$ are plotted in Fig. 4.

The method of INS consists of determining the $U(\zeta)$ function from measured $X(\zeta)$ functions as is discussed in detail in Ref. 2. When the provisional assumptions made above are relaxed, $U(\zeta)$ is not simply the state-density function, but is the transition density of the ion-neutralization process as a function of energy ζ and includes state density and transition probability factors as well as possible final-state interactions and many-body effects.

The steps of the INS method are as follows[2]:

(1) Electron energy distributions $X_K(E)$ are recorded both by analog and digital means for ions of two incident energies K_1 (4 or 5 eV) and K_2 (10 eV).

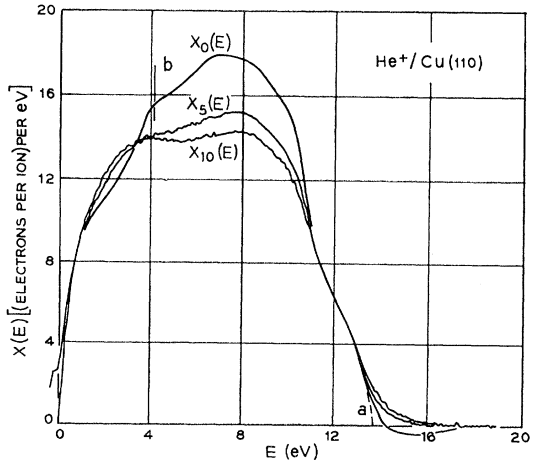

FIG. 5. Graph illustrating the linear extrapolation of $X_K(E)$ distributions to reduce the energy broadening. Experimental analog distributions X_5 and X_{10}, for 5 and 10 eV He^+ ions, respectively, are used. The extrapolated distribution, $X_0=X_5+R(X_5-X_{10})$ with $R=3.11$, is also shown. Only data at $E\gtrsim 4$ eV (E above line b in plot) are used in the subsequent data handling.

[6] H. D. Hagstrum, Y. Takeishi, and D. D. Pretzer, Phys. Rev. **139**, A526 (1965).
[7] H. D. Hagstrum, Phys. Rev. **96**, 336 (1954).
[8] H. D. Hagstrum, Phys. Rev. **122**, 83 (1961).

(2) A linear extrapolation from $X_{K_1}(E)$ and $X_{K_2}(E)$ is made to obtain a distribution $X_0(E)$ for which the broadening due to components which depend on ion velocity is very much reduced, probably to the level of the instrumental energy resolution. This extrapolation is done digitally and makes use of the fact that the energy broadening varies linearly with incident-ion velocity.[2,6] The initial data and the results of such an extrapolation for He^+ ions on atomically clean Cu (110) are shown in Fig. 5.

(3) $X_0(E)$ is now divided by a parametric $P(E)$ function to obtain the internal distribution $F(E)$ and from it the band function $F(\zeta)$ by change of variable from E to ζ. The parameters of $P(E)$ are determined so that the overlapping portions of $F(\zeta)$ obtained for the three ions, He^+, Ne^+, Ar^+, are essentially coincident. $P(E)$ includes all dependences on E, such as final-state density, in addition to the escape probability.

(4) The initial portion of the $F(\zeta)$ function near $\zeta=0$ is further trimmed. This trimming shifts the $\zeta=0$ point by about 0.2 eV from the ζ value at which the extrapolated $X_0(\zeta)$ passes through zero. In some cases, such trimming of $F(\zeta)$ has appeared to be necessary to the successful unfolding of $F(\zeta)$ by means of the step digital unfolding method.[2] We now understand the reasons for this and expect to report our findings elsewhere.

(5) Equation (1) is unfolded sequentially by digital means to obtain $U(\zeta)$ from $F(\zeta)$.

$F(\zeta)$ and $U(\zeta)$ functions for a face each of Cu and Ni are shown in Figs. 6 and 7, respectively. Figures 7 and 8 of Ref. 2 are similar plots for different faces, namely Cu (110) and Ni (111), respectively. The $P(E)$ function, properly placed on the E scale relative to $F(E)$, is also plotted in these figures. Note that the $P(E)$ function is relatively flat over the range of $F(E)$ data used in the unfolding and that it can be approximated very well in this range by the three-parameter function used.

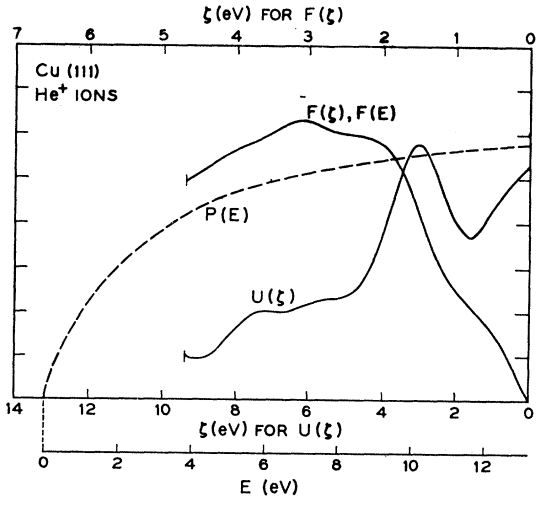

FIG. 6. F, U, and P functions for He^+ ions on Cu (111).

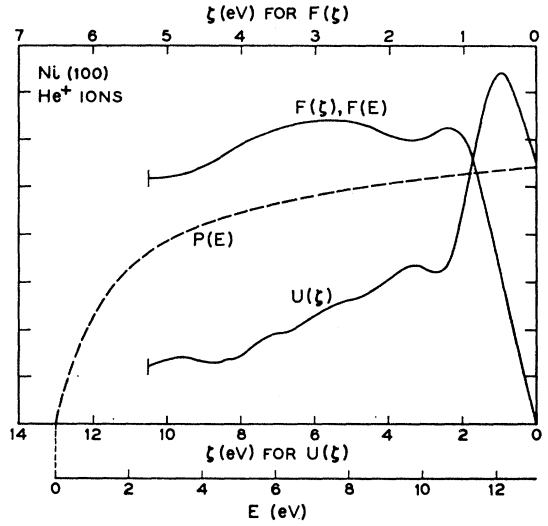

FIG. 7. F, U, and P functions for He^+ ions on Ni (100).

At this point we shall discuss smoothing of the digital data which has been necessary to produce an unfold function $U(\zeta)$ essentially free of "point-by-point" fluctuations or noise. As indicated in Ref. 2, our present computer programs allow for data smoothing at three places in the data-handling procedure. The functions which can be smoothed at these places are: (a) the $X_{K_1}(E)$ and $X_{K_2}(E)$ distributions after the input data have been normalized and interpolated onto the same energy grid, (b) the difference $X_{K_1}(E)-X_{K_2}(E)$ used in the linear extrapolation (step two above), and (c) the extrapolated distribution $X_0(E)$ at the conclusion of step two. In smoothing each of these functions, one can choose from a variety of smoothing formulas, each of which may be used for smoothing over 3, 5, 7, or 9 adjacent data points. All the results presented in this paper have been smoothed at each of these places, thus three times, by the linear formula of simple averaging carried out over 9 adjacent data points, 4 on each side of the data point in question. It is important that these steps in data handling be kept in mind when evaluating the present results and comparing them with other work.

It is clear that the digitalization of the data in itself is a smoothing operation. As is known,[9] this filters out all Fourier components whose wavelengths are less than twice the interval, ΔE, between data points. The effect of 9-point smoothing, in addition to this, is to introduce further filtering of the frequency components.[10] With a single 9-point smoothing, we cannot expect to see features in our data whose extension on the energy scale is appreciably less than $9\Delta E$. This interval on both the

[9] R. W. Hamming, *Numerical Methods for Scientists and Engineers* (McGraw-Hill Book Company, Inc., New York, 1962), Sec. 21.3, pp. 278 ff.

[10] See Ref. 9, Secs. 24.1–24.5, pp. 313 ff.

E scale and the ζ scale for $U(\zeta)$ is 0.9 eV since we have sampled every 0.1 eV. The use of three successive 9-point smoothings spreads the smoothing out over more data points but also has the effect of sharpening the frequency cutoff of the filtering of higher-frequency components in the data. Care has been taken to see that the electronic smoothing also present in the recording of small currents as a function of time is less than the smoothing specifically introduced in the digital data handling.

In the $U(\zeta)$ functions of Figs. 6 and 7, we observe rather rapid changes in slope in regions extending over about 0.5 eV. This observed curvature is consistent with the above discussion and appears to be about the sharpest structure which could conceivably be seen with our present data-handling procedure. We are currently looking into the possibility of obtaining $F(\zeta)$ data of sufficient quality for unfolding with less smoothing. This will require the averaging of $X_K(E)$ curves and possibly closer data sampling. Results to date are promising and indicate that an increase in the resolving power of the INS method can be achieved in this way.

III. EXPERIMENTAL CONDITIONS

The experimental data from which an interpretable $U(\zeta)$ function may be derived must be obtained under the stringent set of experimental conditions catalogued in Sec. IV of Ref. 2. Briefly recapitulated these requirements are: (1) The ions must have low-incident energy to keep the energy broadening inherent in the Auger process relatively small. Ions of 4- or 5- and 10-eV incident energies are used in this work. (2) The energy resolving power of the apparatus in the energy-distribution measurement must be sufficient. It is approximately 0.1 eV at $E=10$ eV. (3) The data must be sufficiently noise-free. (4) The target should be a single crystal whose surface is atomically clean and well-ordered. The first three of these items are apparatus requirements and have been discussed in Sec. IV of Ref. 2. The fourth is specific to the target material studied and must be discussed here in detail for the nickel and copper targets used.

The targets used in this work were cut from single crystals of 99.999% purity, obtained from Research Crystals, Inc., Richmond, Virginia, and Materials Research Corporation, Orangeburg, New York. Initial cuts were made with a rubber-bonded abrasive wheel for the nickel, and with an acid string saw for the copper. Reduction to the desired thickness was done by polishing with abrasives in the case of nickel, and by electrolytic polishing in the case of copper. For all targets, the final polishing was done electrolytically, to remove any mechanically damaged layers. Target dimensions are $7\times14\times0.2$ mm. The targets are spot-welded to tungsten leads with a geometry such that the leads are hidden from the ion beam incident on the front face of the target. Preferential chemical etches were used to remove small amounts of welding-electrode material deposited near the welds. A Pt–Pt-Rh thermocouple is welded to the back of the target at one lead. With these target dimensions, the target can be heated to 800°C by passing a current of about 25 A. After the target was mounted, its alignment and degree of crystal perfection were checked with a Laue back-reflecting x-ray photograph. Orientations within 0.1° of the stated directions. The Laue spots from the central area of the target were very clear and sharp. Low-energy electron-diffraction patterns from the clean target also showed sharp spots, except within about 0.5 mm of the welds at the ends of the target.

The apparatus of Fig. 1 is enclosed in a stainless-steel envelope which is evacuated by both sputter-ion pumps and a mercury-diffusion pump employing two tandem liquid N_2 traps. The entire apparatus including the sputter-ion pumps is baked overnight to 250°C during which interval it is evacuated by the mercury-diffusion pump only. Toward the end of the bake period, with the apparatus at 250°C, all filaments are heated and the sputter-ion pumps are operated repeatedly for short intervals (about 1 min each) until relatively little gas is emitted when the pumps are turned on or off. The sputter-ion pumps are then turned on and left on and cooling of the system begun. When the apparatus has cooled to 150°C the mercury system is isolated by a valve from the main system, its traps are warmed and recooled, after which it is reconnected to the main system. The final stages of cooling of the relatively massive metal system usually occurs during the second night. The use of the mercury system in the manner described was found to reduce both the ultimate pressure and the time required to achieve it. Background pressures achieved in this way are in the range $6\text{–}8\times10^{-11}$ Torr

The target (T in Fig. 1) is cleaned at port 2, the so-called target processing port. Here the sphere Sp may be moved from its retracted position 2 to position 1 where it encloses the target. In this position, the target projects slightly past the outside edge of a shield frame Sh which shields it from evaporation products from the filaments Fi. Ne or Ar gas is admitted to the system to a pressure of 2.5×10^{-2} Torr for sputtering the surface of T. An arc is struck between the electron emitting filaments Fi and the ring R. The arc runs at about 40 V and 25 mA. The shield Sh is held at the potential of Fi. During sputtering the target potential is approximately 100 V negative relative to the plasma potential. The ion current to the target under these conditions is about 1 mA (0.5 mA/cm^2). Sputtering in this way for one minute will remove about 100 monolayers. After sputtering, the target may be annealed by passing current through it. The usual annealing temperature was 600–800°C for both Cu and Ni.

The two principal diagnostic tools used in this work for monitoring the cleanness of the target surface are low-energy electron diffraction (LEED) and the ion-

neutralization results. The latter includes both the form of the kinetic energy distribution $X_K(E)$ of ejected electrons and total yield of such electrons, γ. The use and relative sensitivity of these tools are illustrated by a typical sequence of events for which Fig. 8 gives $X_K(E)$ distributions and Fig. 9 LEED patterns.

The data of Figs. 8 and 9 relate to the Ni (100) target. Curve a of Fig. 8 is the $X_{10}(E)$ distribution for He^+ ions of 10-eV incident energy when the target surface was not clean. The relevant previous history of the target up to this point is as follows: The target had been clean as judged by the criteria given below, had then been exposed to room air for four days, heated for two hours during a subsequent bake-out, and was then not heated during the period of cooling the apparatus. The LEED pattern of Fig. 9(a) was obtained with the target in this condition. Note the fuzzy spot centered in the unit mesh of the clean surface. $X_{10}(E)$ was then changed from curve a to curve c of Fig. 8 by sputtering off 100 layers and by heating the target to 600°C followed by immediate cooling. The LEED pattern also changed from that of Fig. 9(a) to that of Fig. 9(b). Although curve c of Fig. 8 when compared with later results indicates that the target surface is not yet clean, the LEED pattern of Fig. 9(b), taken under the same conditions is essentially indistinguishable from that of the finally clean surface. Curve b of Fig. 8 was obtained after the target had been exposed at room temperature to the residual gases in the apparatus for 42 h. However, the LEED pattern continued to look like that of Fig. 9(b). After a number of additional cycles of sputtering and annealing the $X_{10}(E)$ distribution reached the limiting form of curve d of Fig. 8 with

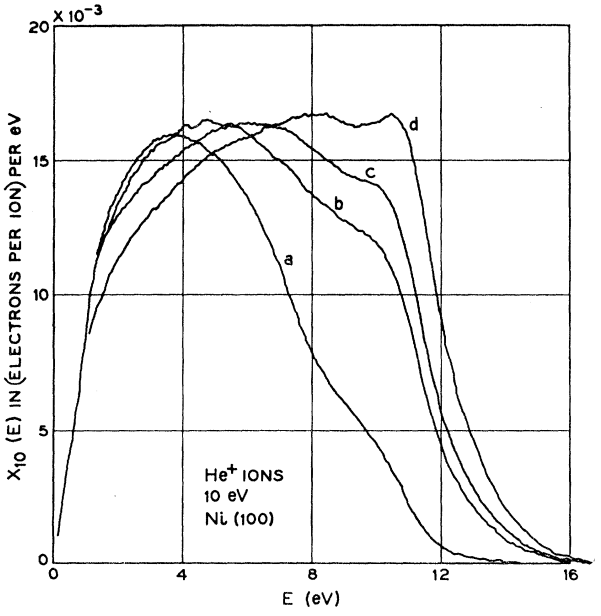

FIG. 8. $X_{10}(E)$ distributions for Ni(100) in various stages of cleanness as discussed in the text.

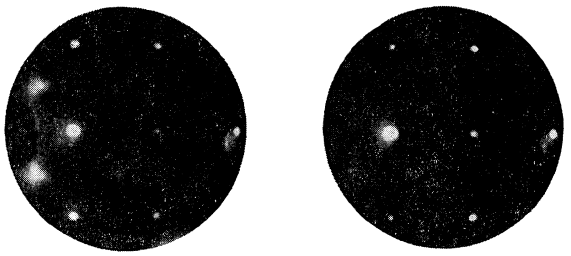

FIG. 9. LEED patterns correlated to $X_{10}(E)$ distributions of FIG. 8 as discussed in the text.

the LEED pattern continuing to be that of Fig. 9(b). Curve d of Fig. 8 was also recoverable by sputtering and annealing after heavy exposure to oxygen (about 10^{-2} Torr sec).

We consider the surface to be clean if (1) it yields a terminal electron-energy distribution $X_K(E)$, after a number of cycles of sputtering and annealing, (2) the terminal $X_K(E)$ is recoverable after heavy oxygen exposure, and (3) the LEED pattern shows no evidence of superstructure spots. We conclude that the Ni (100) surface corresponding to curves c and b of Fig. 8 had amorphously held gas on it which was readily detectable in the ion-neutralization results but not in the LEED pattern. We do not preclude the possibility that careful measurement of the profile of a diffraction spot might show the effect of amorphous surface gas. Spot intensity versus electron energy was not measured in this work but such a measurement for tungsten to be reported elsewhere was found not to change on the adsorption of an amount of amorphously held surface gas easily detected by change in the $X_K(E)$ distribution.

The rate of contamination from adsorbable impurity gases of a clean target can be judged by repeated measurements of the $X_K(E)$ distribution without cleaning of the target between runs. All data reported here were taken under conditions such that the second distribution differed from the first by no more than 1% at any point. It was easy to do much better than this for copper which is relatively unreactive to the gases present in the apparatus. The question of how much degradation is present in the first measured $X_K(E)$ is answered by the flash filament experiment using the Fi filaments as described below.

Another parameter of the ion-neutralization measurements which is easy to measure and generally varies with surface condition is the total electron yield γ, expressed in number of electrons of all energies per incident ion. In some cases it is found not to be a good parameter when the changes in form of $X_K(E)$ accompanying surface contamination are such as to produce little change in γ, the area under the $X_K(E)$ curve. This was not the case in Ni and Cu, and γ is a convenient indicator of the state of the surface. Curve a in Fig. 10 shows the variation of γ with "cold time," t_c,

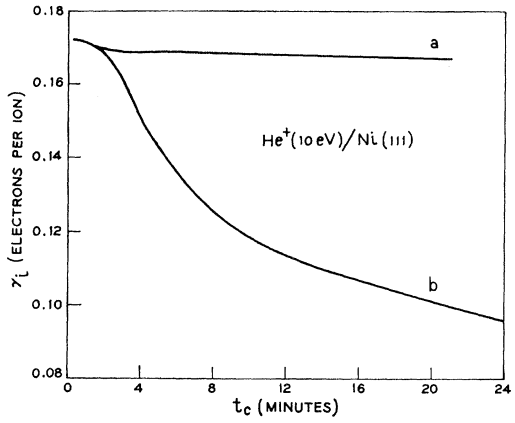

FIG. 10. Plots of total electron yield for He^+ (10 eV) on Ni (111) as a function of "cold time" t_c. Curve a is for present work, curve b for an earlier experiment (Ref. 5).

after a flash of the Ni (111) target to 600°C. t_c is measured from the instant the target heating current is turned off. Thus the target is cooling during the first minutes of the abscissa scale. In the present experiment, the target which was at 600°C at $t_c=0$ has reached 290°C at 1 min, 205°C at 2 min, 160°C at 3 min, and 135°C at 4 min. Note that after this initial cooling period, γ changes very slowly with time indicating a very low concentration of background gases which are adsorbable on this nickel face. For comparison, curve b of Fig. 10 gives the similar curve obtained in the earlier experiment of Takeishi and Hagstrum[5] (their Fig. 6). Note the large improvement in vacuum conditions obtained in the new apparatus. In the earlier work the target cooled somewhat more slowly (see Fig. 2 of Ref. 5), which helped to keep the target clean during the duration of the $X_K(E)$ measurement. The interaction with background gas of any of the faces of copper used in the present work was considerably less than that shown by curve a of Fig. 10 Ni (111). It was found that under our usual experimental conditions, the $X_K(E)$ distributions (and hence γ) was virtually unchanged for Cu during 16 h of exposure to background gases following surface cleaning.

A rigorous check on the possible surface contamination present when the first $X_K(E)$ distribution is measured after target cleaning was made by the following flash filament experiment. A sputtering period is concluded by turning off the tungsten arc filaments, Fi in Fig. 1. This begins a so-called cold interval for these filaments which extends through the period of pumping out the sputtering gas to the conclusion of the measurements necessary to obtain an $X_K(E)$ distribution. During this period, which is normally about 8 min long, both the tungsten filaments Fi and the target T are exposed to the adsorbable gases in the sputtering gas, in the background gases, and in the parent gas from which the ion beam is formed. The initial pressure of the sputtering gas (Ne) is 2.5×10^{-2} Torr. The pressure of the parent gas (He, Ne, or Ar) in the target chamber, which communicates with the ion-source chamber only through a narrow slit, is 2×10^{-7} Torr. At the end of the cold interval, the filaments Fi are flashed to high temperature (>2000°C) and the ballistic pressure rise Δp observed. Δp is calibrated in terms of N_2 monolayer coverage by measuring the Δp versus Δt_c curve with N_2 admitted to the apparatus. In this way we have shown that at the conclusion of an experimental run made on an atomically clean target surface the W filaments Fi have adsorbed less than 2% of an equivalent nitrogen monolayer. Because Ni and Cu are considerably less reactive to the common gases than is W, this should yield an upper bound for the target contamination at the end of the experimental run. Flash-filament measurements of this type are made routinely as a check on the vacuum conditions.

IV. INS RESULTS FOR NICKEL

The five steps of the INS procedure outlined in Sec. II have been applied to the experimentally determined $X_K(E)$ energy distributions. Since these have been discussed in detail in Ref. 2 for one face each of Cu and Ni, we shall show the results for three faces of each metal beginning with the results of step 4. In Fig. 11 the $F(\zeta)$ functions for the clean (100), (110), and (111) faces of nickel are given. These curves result from the extrapolation procedure (step 2), the division by the escape probability (step 3) and the trimming of the high-energy tail which becomes the initial portion of the curve on the ζ scale. The origin of these curves in the experimental $X_K(E)$ functions of Fig. 3 is apparent.

Using digital data for the $F(\zeta)$ functions, the integral of Eq. (1) has been unfolded by the step-digital-unfold method of Ref. 2 to get the transition density function

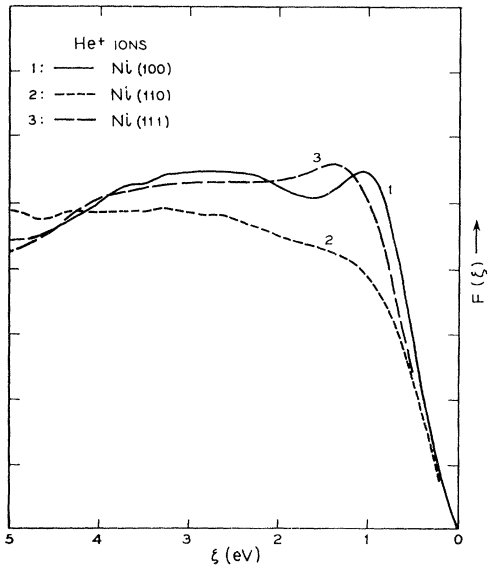

FIG. 11. $F(\zeta)$ functions for He^+ ions on three faces of nickel.

$U(\zeta)$. The results for the three nickel faces (100), (110), and (111) are shown in Fig. 12, as curves 1, 2, and 3, respectively. Although the curves for the three faces generally resemble one another, we see that there are experimentally significant differences between them. Results for the Ni (111) face have been obtained for Ne^+ ions and agree with those presented here for He^+ ions. The results have been published in Fig. 10 of Ref. 2 and discussed there. Shown also in Fig. 12, curve 4 is a $U(\zeta)$ function, U_{av}, which is a weighted average of the three experimental functions for the (100), (110), and (111) crystal faces. Using U_{100}, U_{110}, U_{111} to designate the $U(\zeta)$ function for the three faces, U_{av} is written as

$$U_{av}=(1/26)[6U_{100}+12U_{110}+8U_{111}]. \quad (2)$$

This equation weights the experimental U functions according to the relative frequency of occurrence of equivalent crystal faces. U_{av} is useful in simplifying the comparisons with other data made in Sec. VI.

INS should be able to detect the spin-exchange splitting in nickel if it is larger than a few tenths of an electron volt. Consequently $X_3(E)$ distributions were measured above and below the Curie point. Because the target had to be heated by passing current through it, it was not possible to use the negative feedback stabilization on the ion beam.[4] For this reason measurements were restricted to a narrower energy range near the high-energy end of the $X_3(E)$ distribution. This was sufficient to include the whole of the d-band peak in the nickel data, however. Results for $U(\zeta)$ above and below the Curie point of Ni are shown in Fig. 13. Since the d-band peak should be narrower by the spin-exchange splitting for the curve taken agove the Curie point, we conclude that the amount of the splitting can be no greater than the minimum difference in peak width detectable by the INS method. This difference we estimate to be of the order of a few tenths of an electron volt.

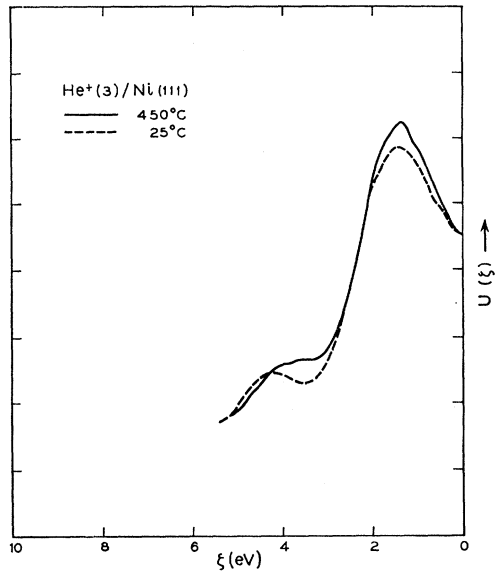

FIG. 13. $U(\zeta)$ functions for 3-eV He^+ ions on Ni (111) derived from data taken with the target at temperatures above and below the Curie point of nickel.

V. INS RESULTS FOR COPPER

The INS results for copper are shown in Figs. 14 and 15. Figure 14 gives $F(\zeta)$ after step 4 of the INS procedure. Figure 15 gives the unfold of these functions

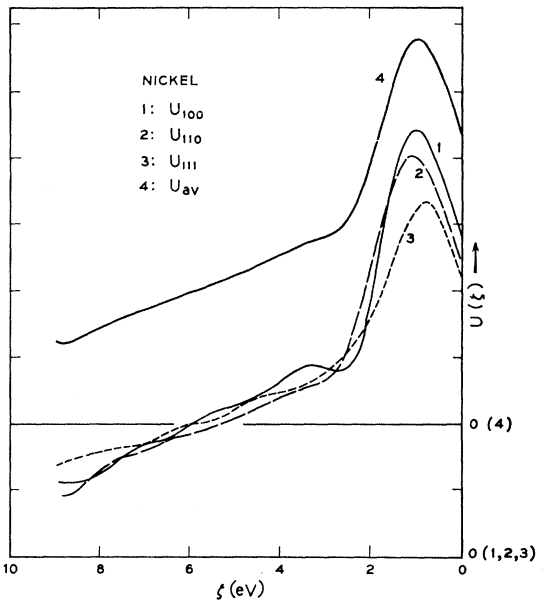

FIG. 12. $U(\zeta)$ functions derived by digital unfolding of the corresponding $F(\zeta)$ functions of Fig. 11.

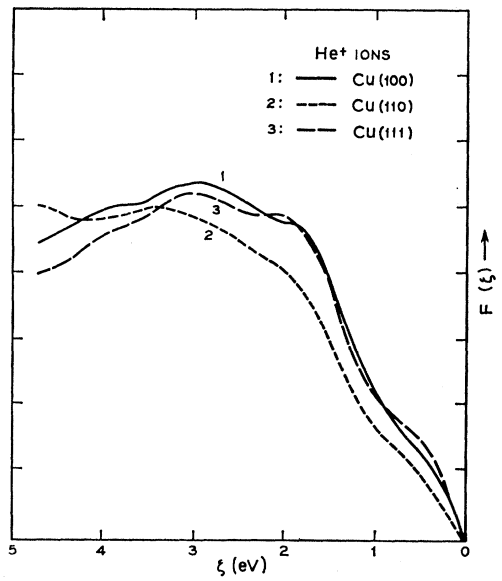

FIG. 14. $F(\zeta)$ functions for He^+ ions on three faces of copper.

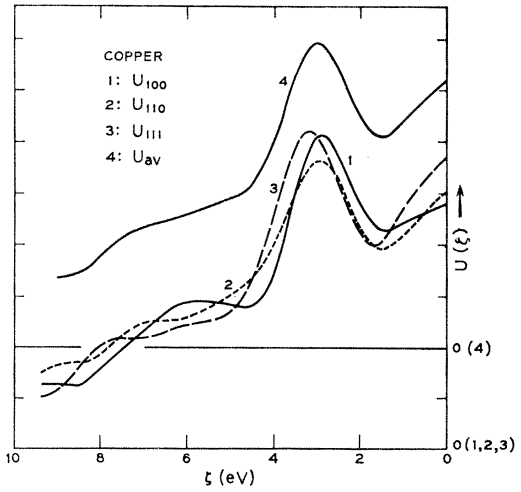

FIG. 15. $U(\zeta)$ functions derived by digital unfolding of the corresponding $F(\zeta)$ of Fig. 14.

to produce $U(\zeta)$ functions by Eq. (1) for each face. Again the results for the three faces are similar, but experimentally significant differences appear. Data for the Cu (110) face obtained using the three ions He^+, Ne^+, and Ar^+ was published in Fig. 9 of Ref. 2. Curve 4 of Fig. 15 is U_{av} calculated from U_{100}, U_{110}, and U_{111} using Eq. (2) as was done for nickel.

A final experimental result concerns evaporation of copper onto a nickel crystal and its removal. This was done as a preliminary test of the evaporator which is part of the target processing port 2 (Fig. 1). Since the results are of interest in themselves and help to establish the quality of the experimental results, we report them here. When copper was evaporated onto the atomically clean Ni (111) face, the $X_5(E)$ distribution changed from the curve shown in Fig. 16, which is characteristic

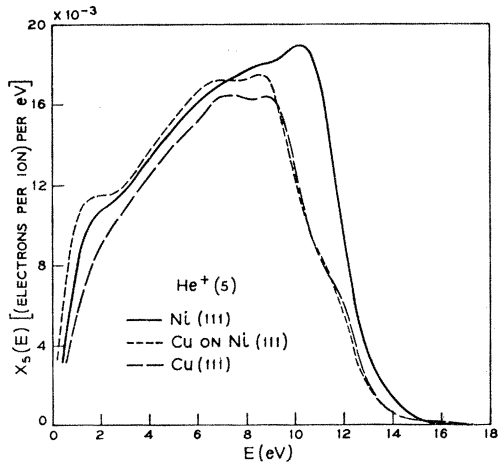

FIG. 16. $X_5(E)$ distributions illustrating changes accompanying evaporation of about 20 layers of Cu onto a clean Ni (111) surface. Curves are shown for clean Ni (111), the starting crystal face, for the Cu film on Ni (111), and for the clean Cu (111) face of a copper monocrystal.

of the clean Ni (111) face, to that labeled Cu on Ni (111). Accompanying LEED photographs showed no change in the LEED pattern except that the spots became somewhat less sharp. From the steps required later to remove the copper film we estimate that its thickness was of the order of 20 atom layers. The $X_5(E)$ distribution for this copper film on nickel is compared in Fig. 16 with that for the atomically clean (111) face of a copper single crystal. Although the difference between these curves is much larger than that encountered in reproducing results for the same surface, it is clear that in every significant particular we are looking at the Cu (111) surface in the case of the copper film.

It was then possible to remove the Cu film and return to the distribution for the atomically clean Ni (111) face. This was accomplished by a series of four sputterings of 1, 2, 2, and 4 seconds duration without accompanying annealing, removing a total of about 20 atom layers, followed by heating of the target in short-duration flashes to 300, 600, and 1000°C. Some change in $X_5(E)$ toward the clean Ni distribution was observed after each step in this procedure. The target surface had been restored a significant fraction of the way back to the clean nickel surface by the end of the fourth sputtering with no annealing. Final achievement of the $X_5(E)$ for clean, annealed Ni (111) by the three short-temperature flashes may have been the result of one or both of the following effects: (1) annealing of the surface layers of the crystal involving release of Ne atoms imbedded there during sputtering, and (2) diffusion of Cu atoms from the surface of the nickel crystal into its bulk.

VI. DISCUSSION OF INS RESULTS AND COMPARISON WITH OTHER WORK

In this section we shall discuss the INS results and compare them with experimental results from the soft x-ray spectroscopy (SXS), the photoelectron spectroscopy (PES), the measurement of optical constants, and theory. It is intended that this discussion should complement that of Ref. 2 where results for one face each of Cu and Ni were used to illustrate the INS method. We shall restrict ourselves to comparisons with those other data which can be used to obtain a transition density for the filled bands. The one exception is the onset of optical interband transitions in copper which relates to one feature of the INS transition density function, namely the position of the top of the d bands.

The INS results for Ni and Cu to be discussed and compared with other work concern (1) the density-of-states structure of the d bands, (2) the s-p bands with particular reference to the deep-band resonances observed by PES, and (3) the exchange-splitting in Ni. The data from other sources are included in Figs. 17–22. The SXS spectra, PES spectra, and theoretical

d-band state density are designated in this paper as $I(\zeta)$, $\rho_P(\zeta)$, and $N_d(\zeta)$, respectively. As a single curve representative of the INS results, we use $U_{av}(\zeta)$ in Figs. 17 and 18. In Figs. 19–22, we plot all three of our experimental $U(\zeta)$ functions for different faces.

For Ni, the SXS result, $I(\zeta)$, in Fig. 17 is the $M_{2,3}$ spectrum recently published by Cuthill, McAlister, and Williams.[11] As pointed out by Cuthill *et al.*, the $M_{2,3}$ emission spectrum agrees well with previous SXS results[12,13] but shows structure on the higher ζ side of the d-band peak not observed in earlier work. The placement of the $M_{2,3}$ spectrum relative to the Fermi level ($\zeta=0$) was made by Cuthill *et al.*, from the inflection point of the x-ray absorption spectrum to an estimated accuracy of a few tenths of an eV.

In Fig. 18 two $I(\zeta)$ functions are shown for Cu. These are the M_3 soft x-ray spectrum derived by Bedo

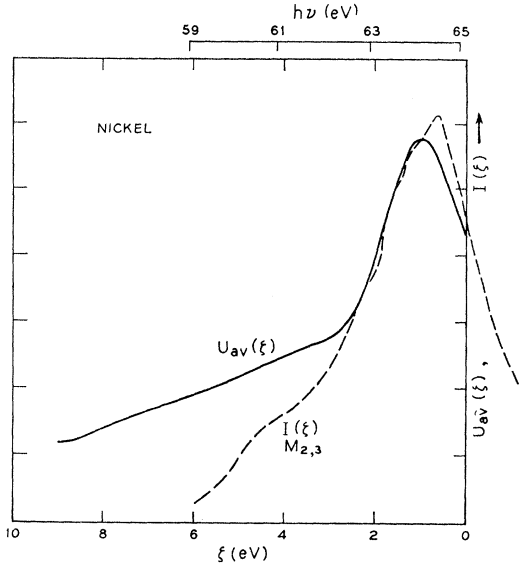

FIG. 17. Graph in which the average function $U_{av}(\zeta)$ derived from data for the three nickel faces is compared with the $M_{2,3}$ soft-x-ray emission spectrum, $I(\zeta)$, obtained by Cuthill, McAllister, and Williams (Ref. 13). $U_{av}(\zeta)$ and $I(\zeta)$ are normalized to approximately the same height.

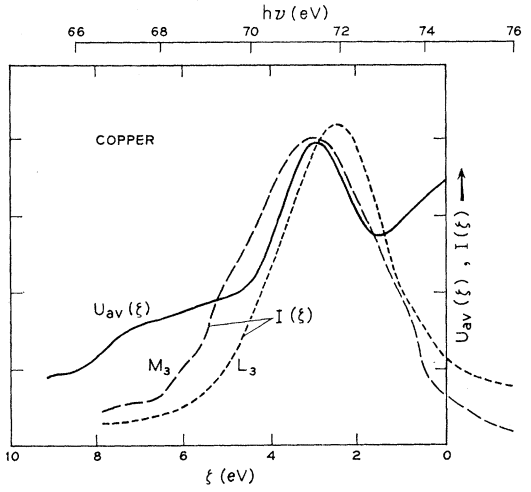

FIG. 18. Graph comparing $E_{av}(\zeta)$ for copper with the M_3 SXS emission spectrum derived by Bedo and Tomboulian (Ref. 16) and with the L_3 spectrum of Cauchois and Bonnelle (Ref. 17). The placement of the SXS spectra on the energy scale is discussed in the text. The $I(\zeta)$ curves and $U_{av}(\zeta)$ are normalized to approximately the same over-all height.

[11] J. R. Cuthill, A. J. McAlister, and M. L. Williams, Phys. Rev. Letters **16**, 933 (1966).

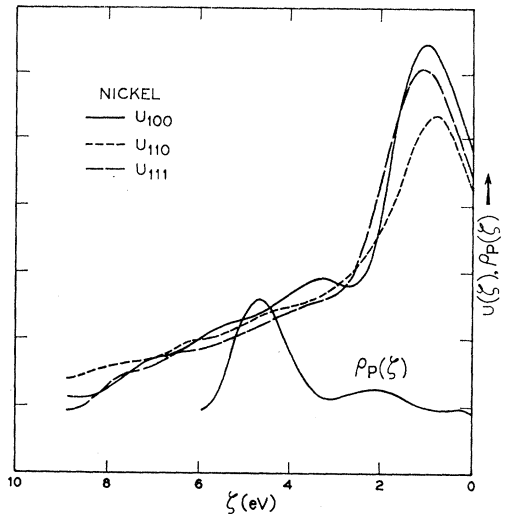

FIG. 19. Graph comparing U_{100}, U_{110}, and U_{111} for nickel with the PES function we have designated $\rho_P(\zeta)$ obtained by Blodgett and Spicer (Ref. 12). No normalization has been made between the INS and PES curves.

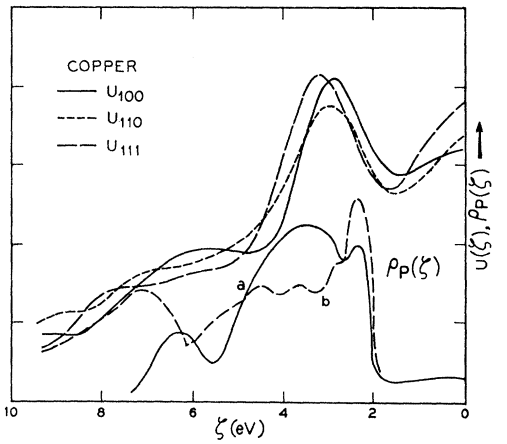

FIG. 20. Graph comparing U_{100}, U_{110}, and U_{111} for copper with two PES $\rho_P(\zeta)$ functions. Curve a is that derived by Berglund and Spicer (Ref. 11) and Berglund (Ref. 19) from PES measurements at lower photon energies on cesiated copper film. Curve b is $\rho_P(\zeta)$ derived by Krolikowski and Spicer (Ref. 20) from PES data at higher photon energy on a copper film without cesiation. No particular normalization between INS and PES curves has been made.

[12] D. H. Tomboulian and D. E. Bedo, Phys. Rev. **121**, 146 (1961).

[13] J. Clift, C. Curry, and B. J. Thompson, Phil. Mag. **8**, 593 (1963).

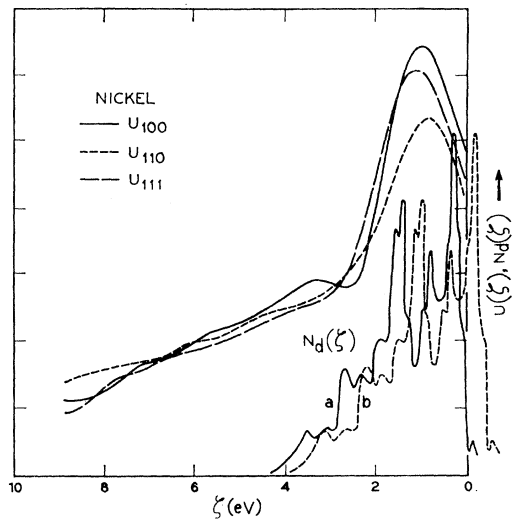

FIG. 21. Graph comparing U_{100}, U_{110}, and U_{111} for nickel with Mueller's theoretically derived state density $N_d(\zeta)$ for nickel d bands ($d_0=7.20$ eV, Ref. 21). No specific normalization between INS and the theoretical curves has been made. The two curves, a and b, are for the bands with opposite spin orientations. Curve b for minority spin orientation has been drawn to the same height as that for majority spin orientation (curve a) and shifted by 0.4 eV (see text).

and Tomboulian[14] by decomposition of their $M_{2,3}$ data and the L_3 soft x-ray spectrum of Cauchois and Bonnelle.[15] There is some ambiguity concerning the location of the M_3 emission edge in the paper of Bedo and Tomboulian who at one point say that an approximate extrapolation places the M_3 emission edge at 74.9 eV but later say that "the onset of absorption at 74.4 eV agrees very well with the M_3 emission edge at 74.6 eV." The M_3 curve in Fig. 18 has been placed on the assumption that the emission edge is at 74.4 eV.

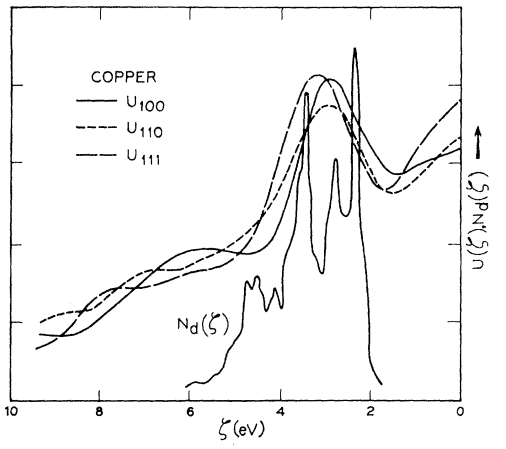

FIG. 22. Graph comparing U_{100}, U_{110}, and U_{111} for copper with Mueller's theoretical $N_d(\zeta)$ for copper d bands ($d_0=5.84$ eV, Ref. 21).

[14] D. E. Bedo and D. H. Tomboulian, Phys. Rev. **113**, 464 (1959).

[15] Y. Cauchois and C. Bonnelle, in *Proceedings of the International Colloquium on Optical Properties and Electronic Structure of Metals and Alloys, Paris, 1965* (North-Holland Publishing Company, Amsterdam, 1966), p. 83.

Cauchois and Bonnelle state in the discussion after their paper that the maximum of their spectrum lies 2.6 eV below the Fermi level. Here ϵ_F has apparently been located by the point of inflection of the L_3 absorption edge as done by Cuthill *et al.*, for Ni.

In Fig. 19 the $\rho_P(\zeta)$ function for Ni is that of Blodgett and Spicer.[16,17] The PES results in Fig. 20 are the $\rho_P(\zeta)$ distributions derived by Berglund and Spicer[17,18] for cesiated Cu, including the peak below the d band recently discussed by Berglund[19] (curve a), and more recently derived by Krolikowski and Spicer[20] for Cu without Cs coverage (curve b).

The theoretical state densities, $N_d(\zeta)$, in the d bands of Ni and Cu chosen for Figs. 21 and 22 are those calculated by Mueller.[21] Similar multipeaked, d-band density functions with prominent peaks near the top and bottom of the band have also been obtained using interpolation schemes by Hodges, Ehrenreich, and Lang[22] and by Wakoh and Yamashita.[23] Either of these would have been equally appropriate here for comparison with our INS results. For the purposes of constructing Fig. 21, we have used an exchange splitting of about 0.4 eV in ferromagnetic Ni.

Now we make three general observations concerning the nature of the experimental and theoretical results we are comparing. First, we should recognize that the end result of PES and SXS, as well as INS, is a transition density function containing state density, matrix element and final-state interaction factors. The SXS spectra, $I(\zeta)$, are usually given as radiation intensity versus voltage (wavelength). In PES, a function which we have designated $\rho_P(\zeta)$ is derived from the kinetic-energy spectra in a manner that retains matrix element factors but removes significant features of the final-state density. It is a transition density in the sense in which we have used the term if the final-state density variations are negligible as appears to be the case. $\rho_P(\zeta)$ is the function labeled "density of states" or "optical density of states" in the photoelectric work. Theory, on the other hand, derives a true state-density function without the complication of transition probability factors for any particular electronic process.

A second observation has to do with momentum

[16] A. J. Blodgett, Jr., and W. E. Spicer, Phys. Rev. **146**, 390 (1966); Phys. Rev. Letters **15**, 29 (1965).

[17] W. E. Spicer, in *Proceedings of the International Colloquium on Optical Properties and Electronic Structure of Metals and Alloys, Paris, 1965* (North-Holland Publishing Company, Amsterdam, 1966), p. 296.

[18] C. N. Berglund and W. E. Spicer, Phys. Rev. **136**, A1044 (1964); W. E. Spicer and C. N. Berglund, Phys. Rev. Letters **12**, 9 (1964).

[19] C. N. Berglund, in *Proceedings of the International Colloquium on Optical Properties and Electronic Structure of Metals and Alloys, Paris, 1965* (North-Holland Publishing Company, Amsterdam, 1966), p. 385.

[20] W. F. Krolikowski and W. E. Spicer (private communication).

[21] F. M. Mueller, Phys. Rev. **153**, 659 (1967).

[22] L. Hodges, H. Ehrenreich, and N. D. Lang, Phys. Rev. (to be published); L. Hodges and H. Ehrenreich, Phys. Letters **16**, 203 (1965).

[23] S. Wakoh and J. Yamashita, J. Phys. Soc. Japan **19**, 1342 (1964).

selection or weighting inherent in $I(\zeta)$, $\rho_P(\zeta)$, $U(\zeta)$, and $N_d(\zeta)$. INS has been applied to single crystals and will yield a transition density weighted heavily in favor of initial and final states whose k vectors are more or less perpendicular to the crystal face used.[2,24] SXS and PES in the particular works cited yield transition densities more nearly averaged over the Brillouin zone, since polycrystalline samples were used. The theoretical $N_d(E)$ functions are specifically averaged over the Brillouin zone. The U_{av} function of Eq. (2) is a step in the direction of deriving a more nearly isotropic transition density from the INS results.

A final consideration is energy resolution. Here one should distinguish between degradation of energy resolution brought about by the inherent energy broadenings of the electronic-transition process and the degradation introduced by the method of measurement and the mathematical processing of the data. It is evident that the 9-point smoothings used in processing the present INS results (Sec. II) will preclude observation of the final detail shown in the theoretical $N_d(\zeta)$ in Figs. 21 and 22. In the future, we expect to reduce the need for mathematical smoothing by averaging $X_K(E)$ curves, and thereby increase the energy resolution of the INS method. For the results discussed in this paper, those derived from PES and SXS exhibit a greater energy resolution than those from INS.

Significant features of the INS results for the d bands in Ni and Cu may be listed as follows:

(1) The expected d bands are observed for both Ni and Cu above a background due to s and p states. The widths and positions of the d bands for the two metals are related to one another according to the rigid-band model.

(2) The d-band peaks measured for targets whose surfaces have differing crystallographic orientations differ in position and width. These differences are well outside the limits of experimental error and are real effects due to the weighting of momentum states normal to each crystal face used. We note that the d peaks in U_{100}, U_{110}, and U_{111} bear essentially the same relationship to each other for Ni as they do for Cu. Thus for each metal the measured d-band states in U_{111} lie farthest from the Fermi level. The d-band peak in U_{110} is essentially coincident with the d peak in U_{111} at its high-energy (low-ζ) side and has a more sloping low-energy (high-ζ) side extending deeper into the band than does the peak in U_{111}. These agreements between the results for Cu and Ni, which can also be seen in the $F(\zeta)$ functions of Figs. 11 and 14, constitute a detailed confirmation of the rigid-band model. Another feature in the results for nickel most likely attributable to a d band is the small peak in U_{100} at $\zeta \sim 3.5$ eV. A similar but broader structure appears in U_{100} for copper.

(3) For copper the INS results show the top of the d bands to lie about 1.8 eV below the Fermi level.

(4) The d-band intensity in the INS transition density function $U(\zeta)$ is much smaller with respect to the s-p band intensity than is expected from the known numbers of electrons in each band. This is evidence of a symmetry-selection rule for INS which expresses the fact that the probability of tunneling into the ion well is much less for d-wave functions than for s- or p-wave functions and has been discussed extensively in Ref. 2.

(5) The good agreement obtained among the INS transition densities derived from data for He^+, Ne^+, and Ar^+ ions, as discussed in Ref. 2, requires that the observed structure in the $U(\zeta)$ function results essentially entirely from initial-state structure, which is constant in position on our ζ scale, and not from final-state structure, which is constant on our E scale (Fig. 4).

The comparisons of the d-band peaks seen by INS and SXS (Figs. 17 and 18) lead to the following conclusions. The positions of the d-band maxima in $U_{\text{av}}(\zeta)$ appear to be in reasonable agreement with the positions of the d peaks in the $I(\zeta)$ from SXS seen in Figs. 17 and 18. As to widths of the d bands, however, it is not really clear how comparison between $U_{\text{av}}(\zeta)$ and the SXS spectra should be made. Cuthill *et al.*,[11] normalized their $M_{2,3}$ spectrum to the same over-all height as the INS result for Ni (111) and consider SXS and INS to agree rather well. However, in the case of the M spectrum, the d band sites on a background of s electrons only, which, since there is no transition probability factor favoring s electrons as in INS, should be a considerably smaller fraction of the d-band intensity than is observed in INS. It thus appears that normalization of $U_{\text{av}}(\zeta)$ and $I(\zeta)$ by equating the heights of the d bands above their respective backgrounds, rather than by equating the over-all heights of the spectra, would reveal the SXS d bands, particularly for Cu, to be wider than the INS d bands.

Cuthill[25] has recently separated the M_3 spectrum for Ni from the M_2 component and finds its d-band width to be somewhat less than that published for the combined $M_{2,3}$ spectrum.[11] He has also compared his Ni-M_3 spectrum with the resolved Cu-M_3 spectrum of Bedo and Tomboulian[14] and finds that the Ni peak is, if anything, wider than the Cu peak especially when the somewhat greater s-band contribution to the Cu result is taken into account. It is Cuthill's opinion that the normalization question raised here will not seriously affect the apparent agreement of the SXS and INS results for nickel.

The comparisons made in Figs. 19 and 20 of d-band structure in the INS and PES results indicate the following. Considering the differences in what each method measures and the relative energy resolutions there is good general agreement between INS and PES for Cu but not for Ni. In fact, when all the evidence is considered, including the theoretical calculations, the one result which appears to be out of line with the others is the PES result for nickel. As Blodgett and Spicer[16,17] point out, the Ni result cannot be derived from the Cu

[24] V. Heine, Phys. Rev. **151**, 561 (1966).

[25] J. R. Cuthill (private communication).

PES result by use of the rigid-band model. In view of the INS and theoretical results for Cu and Ni which seem to confirm the rigid-band model (Figs. 21 and 22), it now appears that the photoelectric spectrum for Ni should also show a d band placed with its maximum energy near the Fermi level and having structure similar to that found by Krolikowski and Spicer[20] for copper reproduced here in Fig. 20.

In Figs. 21 and 22 the comparisons of INS with Mueller's theoretical results show that INS has not resolved the narrow peaks of the theoretical curve. This is undoubtedly due in part to the relatively coarse energy resolution of the INS method as used with 9-point data smoothing. However, as discussed earlier, it must be remembered that INS and the theory are determining different functions. $N_d(\zeta)$ is an average over the whole Brillouin zone, whereas $U(\zeta)$ for a given face includes momentum selection. This suggests the explanation that the peaks shown in $N_d(\zeta)$ are associated with critical points lying at different points in the Brillouin zone. These are weighted differently in the U_{100}, U_{110}, and U_{111} functions, which accounts for the differences among these functions. In fact, the E-versus-k plots for Cu due to Segall[26] and Burdick[27] show the density of states in the Δ direction, as judged by the flatness and number of E, k curves, to be greater in the interval from X_5 to one eV below X_5 than is the case for the density of states in the Λ or Σ directions over the same energy interval. Thus one would expect the d peak in U_{100} to lie closer to the Fermi level ($\zeta=0$) than it does in either U_{110} or U_{111}. This is seen to be the case in Fig. 15.

Another interesting feature of the INS results when compared with theory is the structure below the principle d peak in U_{100} in both nickel and copper mentioned earlier. It is tempting to relate this to the relatively flat bands in the Δ direction near the symmetry points X_1 and X_3. There is no similar flatness of bands in this energy range in either the Σ or Λ directions. Hence, a contribution to the density of states from these states should be seen in U_{100} and not in U_{100} and U_{111}, as appears to be the case. Further work will be required to establish this interpretation firmly.

Although we shall not attempt to extract numerical information from the U_{100}, U_{110}, and U_{111} distributions presented here, it is instructive to compare them with theoretical estimates for some of the specific energy intervals in copper and nickel. With the exception of Segall's calculation based on an l-dependent potential, there is good agreement among theoretical calculations for copper that the energy separation X_1–X_5 is in the range 3.3 to 3.5 eV[26–29] and that the interval from X_5 to the Fermi level, X_5–ϵ_F, is 1.9 eV.[26,27] Thus a theoretical estimate of X_1–ϵ_F for copper is ~5.3 eV. The $U(\zeta)$ distributions presented here are certainly not in disagreement with these values. The top of the d band, as indicated by a rise in $U(\zeta)$, occurs near 1.8 eV. The theoretical X_1 position (ζ~5.3 eV) puts this point somewhere in the broad low peak below the main d peak in U_{100} for copper.

Theoretical values for the interval X_1–X_5 in nickel range from 4.13–5.25 eV.[28–31] Since X_5 is near ϵ_F, this places X_1 somewhat below the small peak in U_{100} centered at ζ~3.5 eV. We note that Mueller's d bands for nickel obtained by a procedure which starts by fitting to Burdick's copper calculation gives X_1–X_5 ~3.5 eV.

Finally, we may compare our results for the position of the top of the d band with the onset at 2.1 eV of the optical interband structure in the reflectivity of copper observed by Ehrenreich and Philipp[32] and Beaglehole,[33] and discussed by Cooper, Ehrenreich and Philipp[34] and Ehrenreich.[35] Photoelectric emission appears to begin weakly at ζ~1.8 eV and rises rapidly at ζ~2 eV.[20]

It appears that both the optical data and PES give an onset about 0.2 eV or so higher than the INS threshold. This could be interpreted on the basis of the suggestion of Copper, Ehrenreich and Philipp[34] that the phototransitions in both the reflectivity and photoemission experiments occur from the flat, heavy-mass Q_+ band near L_{32} to the Q_- band at the Fermi level near L_2'. The INS threshold for the (100) face on the other hand, in all probability, involves transitions from X_5 to the Fermi level. Thus, the "top" of the d band observed by INS should be closer to the Fermi level than the optical determination by the separation of X_5 from the point on the Q_+ branch at the k value at which the Q_- branch crosses the Fermi level. The calculations of Segall[26] and Burdick[27] indicate that this separation could be about 0.2 eV. Without pressing the accuracy of this consideration too far, it does appear that the INS result is reasonable and that neither the INS method of locating the Fermi level ($\zeta=0$) by extrapolation nor the degradation of energy resolution are introducing any large amount of error.

Our second major comparison of the INS results with other work concerns the broad s-p band on which the d band sits. The INS results in this regard are two. First, $U(\zeta)$ functions for both Cu and Ni do not show any features of appreciable intensity other than the d band. A peak of the magnitude of that found in Ni at $\zeta=4.5$ eV by Blodgett and Spicer[16] (Fig. 19) should easily be detected by our present procedures were it present in

[26] B. Segall, Phys. Rev. **125**, 109 (1962).
[27] G. A. Burdick, Phys. Rev. **129**, 138 (1963).
[28] L. F. Mattheiss, Phys. Rev. **134**, A970 (1964).
[29] S. Wakoh, J. Phys. Soc. Japan **20**, 1894 (1965).
[30] J. G. Hanus, Quart. Progr. Rept., MIT, Solid State and Molecular Theory Group, Cambridge, Massachusetts, April, 1961, p. 2 (unpublished); April, 1962, p. 27 (unpublished).
[31] J. Yamashita, M. Fukuchi, and S. Wakoh, J. Phys. Soc. Japan **18**, 999 (1963).
[32] H. Ehrenreich and H. R. Philipp, Phys. Rev. **128**, 1966 (1962).
[33] D. Beaglehole, Proc. Phys. Soc. (London) **85**, 1007 (1965).
[34] B. R. Cooper, H. Ehrenreich, and H. R. Philipp, Phys. Rev. **138**, A494 (1965).
[35] H. Ehrenreich, in *Proceedings of the International Colloquium on Optical Properties and Electronic Structure of Metals and Alloys, Paris, 1965* (North-Holland Publishing Company, Amsterdam, 1966), p. 109.

the $U(\zeta)$ function. Second, the s-p intensity in $U(\zeta)$ for both Cu and Ni decreases in magnitude with increasing ζ. This is a matrix element effect arising from the decrease in wave-function magnitude at the ion position as ζ increases. Theory[26,27] leads us to expect an s-p band which is roughly constant in density over a broad range.

The more prominent of the deep-band resonances found in the PES work on Ni and Cu is the large peak, centered at $\zeta=4.5$ eV, to be seen in $\rho_P(\zeta)$ function for Ni reproduced in Fig. 19. No evidence of this peak is to be seen in the INS $U(\zeta)$ function making it consistent with the SXS results in this regard and pointing to the conclusion that the resonance must possess characteristics which make it "invisible" to both SXS and INS. Mott[36] has suggested that there is an appreciable admixture of the state $3d^84s^2$ into the many-electron wave function of the ground state of nickel. He views the photoelectric resonance as arising from photoexcitation of a d electron from a nickel atom locally in the $3d^8$ configuration. Such a process is visualized as resulting finally in two holes below the Fermi level and a second electron excited above the Fermi level in addition to the observed photoelectron. On this picture the resonance is in a sense the reproduction of the d band displaced deeper in the band by the energy required to form another electron-hole pair. Mott points out that the charged central core of an atom undergoing the soft x-ray transition would preclude the $3d^8$ configuration on such an atom and hence the observation of the resonance in SXS. He also suggests that a similar discrimination against the $3d^8$ configuration on atoms near the incoming ion in INS is caused by the charge of the ion.[37] Spicer[38] has suggested that the d-wave functions about an atom in the $3d^8$ configuration might, because of the difference in the charge distribution about the atom, be pulled in even closer to the atom than for $3d^9$ and thus make the $3d^8$ configuration essentially invisible in INS by virtue of its discrimination against d versus s or p electrons. Thus INS, like SXS, appears to be consistent with Mott's model but does not provide any positive evidence favoring it.

Another suggestion concerning the PES resonance in Ni is that of Cuthill *et al.*,[11] who view it as the result of a double photoexcitation in which one photoelectron from the d band always makes a highly probable direct transition between specific states and the other d electron uses up the remaining energy of the photon to reach a final state whose energy varies with photon energy. Since this is a suggestion specific to the photoprocess, we see no inconsistency with the INS result but also no specific confirmation of the suggested model.

Finally, there is Phillips's suggestion[39] that the resonance is the result of a concentration of atomic-like states resulting from what he terms "maximal atomic correlation" at the energy of the resonance. The failure of INS to reveal this strong feature requires one or the other of the following conclusions: (1) The k vectors associated with states in this resonance are localized in a direction or directions such that there is insufficient intensity normal to any of the three crystal faces used in the INS experiment. (2) The transition probability of the Auger transitions involving these states is very much less than that for photoelectric excitation. Possibility (1) appears unlikely. As to the second, Phillips[40] has recently suggested that d-d correlation corrections act in opposite directions for optical excitation and INS. In optical excitation, they enhance oscillator strengths, whereas in INS they reduce the transition probability by reducing the magnitude of the "tail" of the complete many-electron probability density at the position of the incident ion. Some such effect is clearly required.

Another feature outside the energy range of the d bands which we should discuss, is the peak near $\zeta=6$ eV which was found in the unfold $U(\zeta)$ of the earliest data taken for copper [Cu (110)] and is to be seen in the first publication of our work in Cu and Ni.[1] We have since studied two other faces of copper [Cu (111), Cu (100)] and in neither did the same small feature appear. This led us to put the original Cu (110) target back into the apparatus and repeat the INS measurements. The curve obtained in this later restudy is that given here and used in Ref. 2. Although this curve reproduces the early d-band evidence very well, it does not show the small peak near $\zeta=6$ eV. In any event, we believe the more recent result on Cu (110) to be the more trustworthy. It agrees with the Cu (111) and Cu (110) data in not revealing a peak of any appreciable magnitude near $\zeta=6$ eV in the INS transition density for Cu.

Our third point of discussion concerns the exchange splitting of nickel. We have seen that our measurements of the nickel d bands above and below the Curie point are consistent with an exchange splitting of no more than a few tenths of an eV. This is in good agreement with the recent general estimate of 0.25 eV made by Herring[41] and the summary value of 0.35 ± 0.05 eV given by Wohlfarth.[42]

ACKNOWLEDGMENTS

We are happy to acknowledge the expert technical assistance of P. Petrovich in operating our relatively complex apparatus. We are grateful also to C. N. Berglund, F. M. Mueller, J. C. Phillips, E. O. Kane, and W. E. Spicer for discussion and critical reading of the manuscript.

[36] N. F. Mott, in *Proceedings of the International Colloquium on Optical Properties and Electronic Structure of Metals and Alloys, Paris, 1965* (North-Holland Publishing Company, Amsterdam, 1966), p. 314.
[37] N. F. Mott (private communication).
[38] W. E. Spicer (private communication).
[39] J. C. Phillips, Phys. Rev. **140**, A1254 (1965).
[40] J. C. Phillips (private communication).
[41] C. Herring, in *Magnetism*, edited by G. Rado and H. Suhl (Academic Press Inc., New York, 1966), p. 144.
[42] E. P. Wohlfarth, in *Proceedings of the International Conference on Magnetism, Nottingham, 1964* (Institute of Physics and The Physical Society, London, 1965), p. 51.

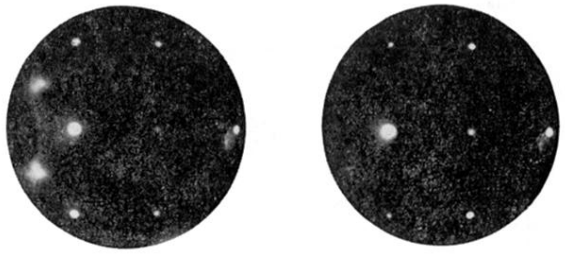

(a) (b)

FIG. 9. LEED patterns correlated to $X_{10}(E)$ distributions of FIG. 8 as discussed in the text.